



Investigating the Microstructure, Hardness and Tensile Behavior of Magnesium AZ80 Alloy and AZ80/SiC Nanocomposite Manufactured Through Dual Equal Channel Lateral Extrusion (DECLLE)

M. A. Salevati¹ · A. Imam¹ · R. Seifi² · F. Akbaripناه³

Received: 14 December 2019 / Accepted: 10 March 2020 / Published online: 30 March 2020
© The Korean Institute of Metals and Materials 2020

Abstract

In this study, first, AZ80 magnesium alloy and AZ80/SiC nanocomposite were manufactured through a stir casting approach. Then built samples underwent five passes of DECLLE process at a constant temperature of 300 °C. Changes in microstructures, hardness, and tensile strength were measured in the annealed alloy and nanocomposites as well as samples with 1, 3, and 5 passes of DECLLE to determine the effects of SiC strengthening nanoparticles and number of the DECLLE passes. Results show that there is a most significant decrease in grain size due to adding the nanoparticles. The microstructure of the initial AZ80 samples made by large grains and inhomogeneous structure with an average grain size of 60.3 μm. After five DECLLE passes for samples with nanoparticles, the structure is turned into fine and homogenous grains with an average size of 4.5 μm. Along with this decreasing trend in the grain size, hardness shows a 20.7% increasing. The results of the uniaxial tensile test show that yield strength and ultimate tensile strength have increased respectively from 74 to 131.8 MPa for initial samples to 113 and 221.9 MPa in nanocomposites. Finally, their values reach to 191.3 and 288.3 MPa after applying five passes of DECLLE process. The results indicate that it is possible to significantly improve the microstructure and mechanical properties of the AZ80 magnesium alloy through enriching by nanoparticles. Using severe plastic deformation processes such as DECLLE can induce a further decrease in grain size and significant improvement in the mechanical properties without causing changes in the samples' dimensions.

Keywords Magnesium-based nanocomposite · SiC nanoparticles · DECLLE process · Mechanical properties · Microstructure

1 Introduction

Magnesium and its alloys, as some of the lightest industrial metals offer unique metallurgical properties such as high strength to weight ratio, high machining, and recycling capabilities, and high dampening capacity, which has resulted in their use in various industries [1, 2]. On the other hand, the

presence of hexagonal closed packed (HCP) crystal structure means that magnesium alloys have low ductility at room temperature because their only active slip planes are the basal planes. Due to its high hardness, AZ80 alloy shows low ductility, and this limitation has become one of the main barriers in expanding its uses. Therefore, any methods capable of covering this limitation will gain increased attention.

One of the most effective methods for improving mechanical properties and expanding the applications of magnesium alloys is the manufacturing of the nanocomposites [3]. Among the magnesium matrix nanocomposites, materials manufactured through the addition of discontinuous reinforcements, especially nanoparticles, not only show improved mechanical properties but offer lower costs, easier processing, and better machining capabilities [4–6].

Ceramic nanoparticles are often used for strengthening metal matrix nanocomposites due to their unique mechanical properties such as low density, high hardness,

✉ A. Imam
aimam@srbiau.ac.ir

¹ Department of Mechanical Engineering, Science and Research Branch, Islamic Azad University, Tehran, Iran

² Department of Mechanical Engineering, Faculty of Engineering, Bu-Ali Sina University, Hamedan 65175-4161, Iran

³ Department of Mechanical Engineering, Faculty of Engineering, Malayer University, Malayer, Iran

high strength, high elasticity modules, suitable thermal stability, and low cost [4]. Among these ceramic nanoparticles, sic. particles are more popular for use in magnesium matrix compared to other ceramics due to their wettability and relatively high stability in molten magnesium [7].

The use of thermomechanical processes is necessary to increase strength, improve the homogeneity of nanoparticle distribution and microstructure and promoting the use of magnesium-based nanocomposites in industries. Physical and mechanical properties of crystalline materials depend on various factors, the most important of which is their average grain size [8]. Although the grain size in commercial alloys can be reduced through the use of suitable thermomechanical processes, these methods can only produce materials with micrometer-sized grains [9]. Today, the main goal of the high-temperature deformations is the manufacturing of materials with nanosized or ultrafine grains, which have unique characteristics such as increased hardness, strength, electrical resistance, thermal conductivity and corrosion resistance [10]. To turn coarse-grained crystalline materials into materials with ultra-fine grains, it is necessary to apply the severe strains. Recently, SPD methods have received more attention as one of the methods for manufacturing of ultra-fine grains without changing the dimensions of the samples [11]. However, there are a few studies about the using of the SPD processes for magnesium-based nanocomposites [12–14].

Nie et al. [13] investigated the effects of multi-directional forging (MDF) process on AZ91 alloy and SiC/AZ91 nanocomposite at a constant temperature. Their results showed a decreasing in average grain size and increasing in the homogeneity of the microstructure after addition of the nanoparticles and MDF process. They reported a 46% and 139% increasing in the ultimate tensile strength, respectively. Furthermore, ductility had also shown a 3.3 times increase.

In a study by Qiao et al. [12], the effects of extrusion and equal channel angular pressing (ECAP) processes on SiC/AZ91 nanocomposite were investigated. In their results, improvement in the microstructure and removal of agglomeration of the nanoparticles were reported when compared to forged samples. They also reported a significant increase in the ultimate tensile strength due to extrusion and then increasing the number of the ECAP passes.

Changes in the microstructures and mechanical properties of AZ91 alloy strengthened using different volume percentages of sic. nanoparticles after closed-cycle die forging (CCDF) process was studied by Liao et al. [14]. Their results indicated a significant decrease in the grain size and higher homogeneity of the grains as a result of decreasing in the process temperature. They stated that an increase in the yield stress (YS) and ultimate tensile strength (UTS) occurs as a result of the nanoparticle addition (Orowan strengthening mechanism),

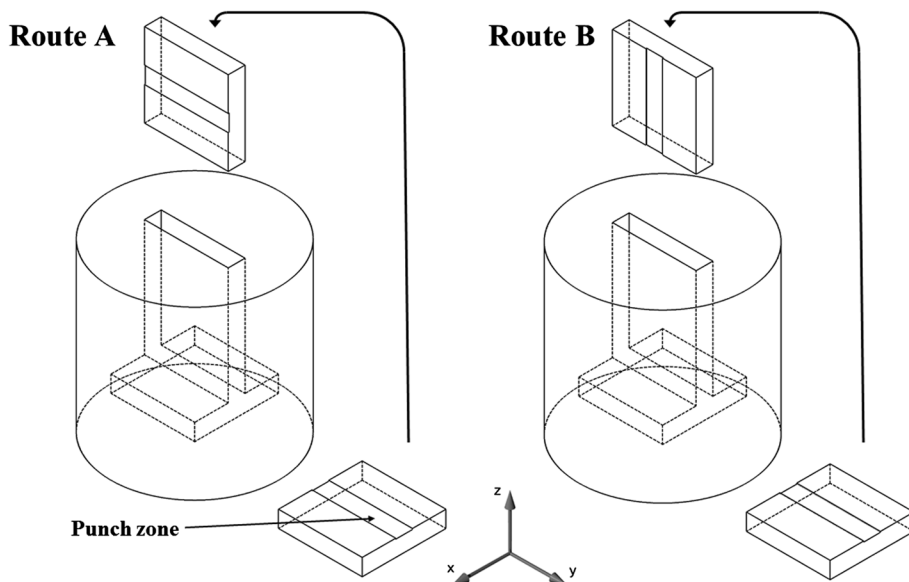
and an increase in the number of CCDF passes continues this increasing trend.

ECAP process is one of the SPD processes whose effects on the magnesium alloys have significantly been investigated due to its ease of use, lack of dependence on advanced equipment, and desirable impact on the microstructures and mechanical properties of the materials [15–17]. DECLC process is one of the novel SPD techniques which is based on a mixture of the ECAP and MDF processes and is known as the only method capable of applying high strains on plates. In this method, the sample, which usually has equal width and length, is first placed in a vertical channel with cross-section equal to that of the sample and is extruded into a horizontal channel which is placed directly under the vertical channel and also has similar dimensions to the sample through pressure applied with a punch. Two walls are placed at the end of the horizontal channel, which limits the flow of the material in the horizontal direction [18]. The advantages of the DECLC compared to ECAP include lower required deformation force, higher effective strain, the possibility of rotating the samples in different directions, and causing more uniform deformations [18–20]. According to Fig. 1, the DECLC process can be carried out in two separate routes as A and B. In route A, after leaving the die, the sample only rotates 90 degrees around its y-axis and again enters through the vertical channel. However, in route B, the sample rotates 90 degrees around its x-axis and then another 90 degrees around its z-axis before reentering in the vertical channel [18].

The DECLC process has not been previously investigated on nanocomposites. Microstructures and mechanical properties of AZ31 magnesium alloy under repeated upsetting (RU) process (which is another name for the DECLC process) were investigated by Guo et al. [20]. Their results indicated that route B results in finer and more homogenous microstructures and higher strength and ductility in comparison with route A due to an extra 90° rotation. The results of the study by Fereshteh-Saniee et al. [21] also showed that five passes of the DECLC process in ZK60 magnesium alloy result in a 93% decrease in grain size and the behavior of samples change from brittle to ductile with an increasing in the number of the passes.

In the current study, first, the effect of adding sic. reinforcement nanoparticles on AZ80 magnesium alloy is investigated. Then, the manufactured nanocomposites undergo the DECLC process, and the results are evaluated. The parameters used in this evaluation include microstructure, average grain size, surface hardness, and tensile strength.

Fig. 1 Schematic illustration of the die and the routes of DECLE process



2 Materials and Methods

In this study, AZ80 magnesium alloy with high purity (approximately 99.9%) and chemical composition of Mg-8.03Al-0.5Zn-0.02Mn was used as the metal matrix. To manufacture the nanocomposite through the stir casting method, a 1.5% volume fraction of sic. nanoparticles with a purity of 99%, with a density of 3.22 g/cm^3 and an average particle size of 50 nm was added to the matrix. To this end, first, molten AZ80 alloy was prepared at $750 \text{ }^\circ\text{C}$ under Magrex 36 flux, and then the wet nanoparticles were gradually added to the molten alloy. To create a homogeneous structure, the molten alloy was stirred for 6 min using a magnetic stirrer. Before pouring the molten alloy, steel dies were preheated to $300 \text{ }^\circ\text{C}$. In order to prepare the casted samples for the DECLE process, samples with dimensions of $50 \text{ mm} \times 50 \text{ mm} \times 10 \text{ mm}$ were prepared through machining. Along with nanocomposite, AZ80 was also cast under the same conditions to investigate the impact of nanoparticle addition. Finally, samples were annealed for 6 h at $400 \text{ }^\circ\text{C}$ to create a more homogeneous microstructure and to reduce the effects of destructive phases.

Annealed nanocomposite samples were fully covered in MoS_2 lubricant before each DECLE pass and were placed in the die at the temperature of $300 \text{ }^\circ\text{C}$ to become fully isothermal. Finally, samples underwent up to 5 passes of the DECLE process at a constant temperature of $300 \text{ }^\circ\text{C}$ using a servo electromechanical testing machine with a maximum capacity of 400 KN. This process was carried out at a constant speed of 2 mm/min and using route B without any obvious cracks in the samples after 1, 3, and 5 passes of the process. Die and samples were heated using heating elements placed at various locations, and their temperature

was kept constant using a thermometer and an automatic temperature control circuit.

The effective strain for each pass of the ECAP process only depends on the angle between two channels (φ) and the concavity angle of the outer layer of the bend between two channels (ψ), which can be calculated using the equation provided by Iwahashi et al. [22]. By assuming $\varphi = 90^\circ$ and $\psi = 90^\circ$ in an ECAP die, the effective strain is calculated as 1.15. However, for the DECLE die, the effective strain for a single pass is estimated to be 1.44 using the upper-bound analysis [19]. Therefore, the effective strain applied to the samples in the DECLE process is 25% higher than that of the ECAP process.

In the DECLE process, the dead zone with the greatest changes in strain forms exactly under the punch. The existence of this zone in samples prepared through this method is one of the disadvantages of the DECLE in compared with the ECAP process. However, at higher passes of the process, since this zone is deformed again, it can be said that all samples become homogeneous [18, 23]. However, in order to prevent possible effects of this zone on the results, all samples used for various tests were selected from areas farther away from the dead zone.

As can be seen in Fig. 2, using wire electrical discharge machining, test samples for the microstructure and hardness tests were selected from the YZ plane, which is the cross-section perpendicular to the extrusion direction. Samples for tensile tests were cut from the XY plane due to the geometrical limitations of the samples. First, the distribution of the nanoparticles and the quality of the stir casting of nanocomposites was investigated using energy dispersive spectrophotometry (EDS) method, and sic. nanoparticles were also examined by transmission electron microscopy (TEM). In order to investigate the microstructures of AZ80

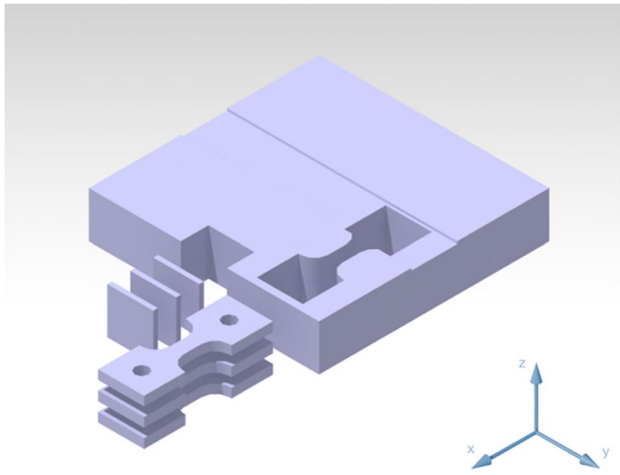


Fig. 2 Schematic geometrical position of microstructure, microhardness and tensile test specimens

alloy, AZ80/SiC nanocomposite, and DECLE nanocomposite samples, were polished and then etched using a solution of 4 g picric acid, 10 mL acetic acid, 10 mL distilled water and 70 mL ethanol. Microstructure images were obtained using a HUVITZ optical microscope, and average grain size was determined using these images and Clemex software. The grain size was calculated using the equivalent circle method, and the distribution graph of grain size was also plotted.

One of the methods used to investigate the homogeneity of the reinforcement particle distributions and to determine the homogeneity level of microstructures is the measurement of surface hardness. To this end, Vickers microhardness of the samples was measured according to ASTM E384 [24] standard and with ILLINOIS-60044 microhardness tester. For each sample, a test sample with dimensions of 10 mm × 10 mm was prepared from cross-section perpendicular to the extrusion direction, and hardness was measured at nine different points with the loading of 100 g for 30 s. The scheme of placement for these 9 points is shown in Fig. 3. It was assured that test locations are placed 2.5 mm away from each other and samples' edges.

The small dog-bone samples for the tensile test were prepared, as shown in Fig. 2 from the XY plane, parallel to the X-axis of the sample. In these samples, the gauge length, width, and thickness were 4, 3 and, 2 mm, respectively. Uniaxial tensile strength test was carried out at room temperature with a strain rate of $1 \times 10^{-3} \text{ s}^{-1}$ using a 50 kN servo electromechanical testing machine. For each stage, three different samples were tested, and their results showed a minimum deviation approximately equal to ± 2 MPa in the YS and UTS values. In order to investigate the fracture surface of the tensile test samples, the fractography was investigated using scanning electron microscopy (SEM).

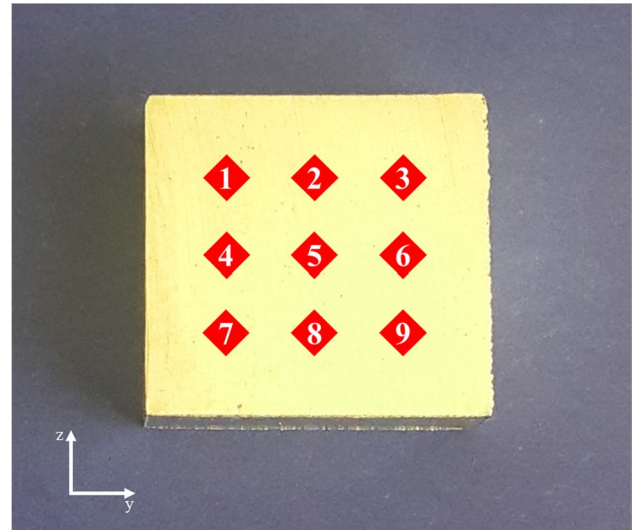


Fig. 3 Schematic representation of selected points to measure microhardness

3 Results and Discussion

3.1 Microstructure Investigations

Microstructure and grain size distribution of the annealed AZ80 alloy and AZ80/SiC nanocomposites after annealing and DECLE passes are shown in Figs. 4 and 5. Figure 4a shows the coarse grain size structure of the AZ80 alloy with an average grain size of 60.3 μm . Figure 5a also shows the presence of an inhomogeneous structure in the AZ80 alloy. Inhomogeneous structures with coarse grain size in AZ80 magnesium alloy were also mentioned in other studies [25, 26]. Figure 4b shows a significant reduction in the grain size to 36.7 μm and improvement in grain size distribution as a result of the addition of a 1.5% volume fraction of the sic. nanoparticles. The sic. nanoparticles present in the grain boundaries act similar to dislocations, and by creating more nucleation sites and facilitating the nucleation of primary inhomogeneous magnesium phase, prevent grain growth. This phenomenon is known as pinning. On the other hand, the nanoparticle addition can reduce the space between particles, resulting in stronger bonds and high energy intersections which are suitable locations for nucleation [25, 27]. Reducing the scattering of the grain size distribution in Fig. 5b also confirms that the nanoparticle addition has resulted in a reduction of the microstructure heterogeneity.

According to Figs. 4 and 5c, after the first pass of the DECLE process, the decreasing trend in the grain size continues at a slower pace, initial coarse grains still being observed next to finer grains, which are built near grain boundaries due to nucleation. This structure is created due to incomplete dynamic recrystallization (DRX) process. The

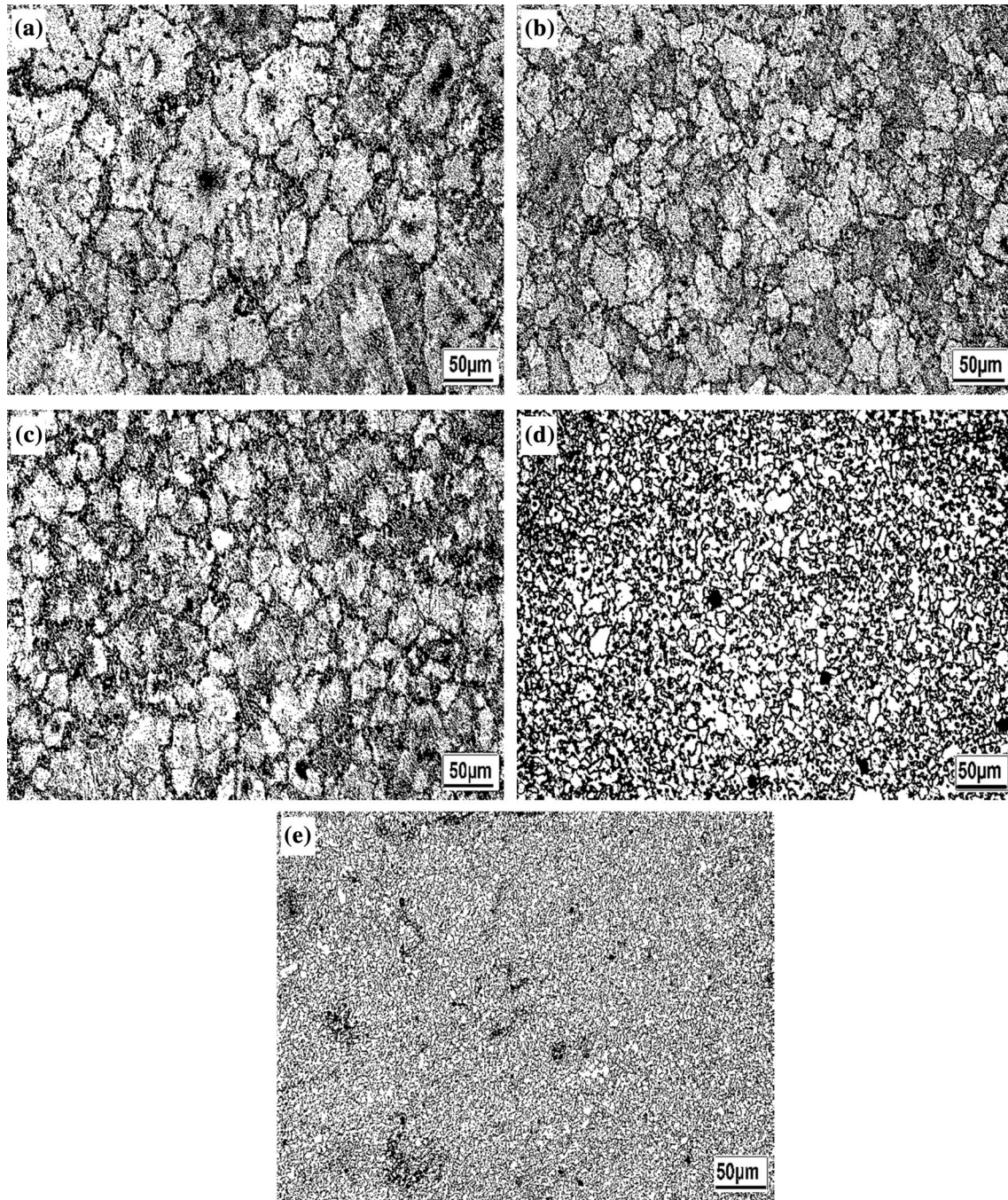


Fig. 4 Optical Micrographs of the **a** Annealed AZ80, **b** Annealed SiC/AZ80, and the SiC/AZ80 after **c** 1, **d** 3, **e** 5 passes of DECCEL

average grain size after the first DECCEL pass is 30.6 μm and Fig. 5c shows that the microstructure of the samples is slowly turning from inhomogeneous to a homogeneous structure and the microstructure is neither coarse-grained nor fine-grained. The presence of bimodal microstructures in the first pass of the SPD processes, as observed in the first pass of DECCEL (Fig. 5c), has also been mentioned in other studies [14, 17, 28]. After the third DECCEL pass, as

shown in Fig. 4d, along with an increase in accumulated strain and progression of the DRX process, the number of coarse grains is minimized, and a large portion of the structure has the fine grains. The average grain size after the third DECCEL pass reduced to 10.7 μm . Figure 5d also shows a more homogeneous structure in comparison with the first pass. Investigating the microstructure of the nanocomposites after the fifth DECCEL pass shows the formation of ultrafine

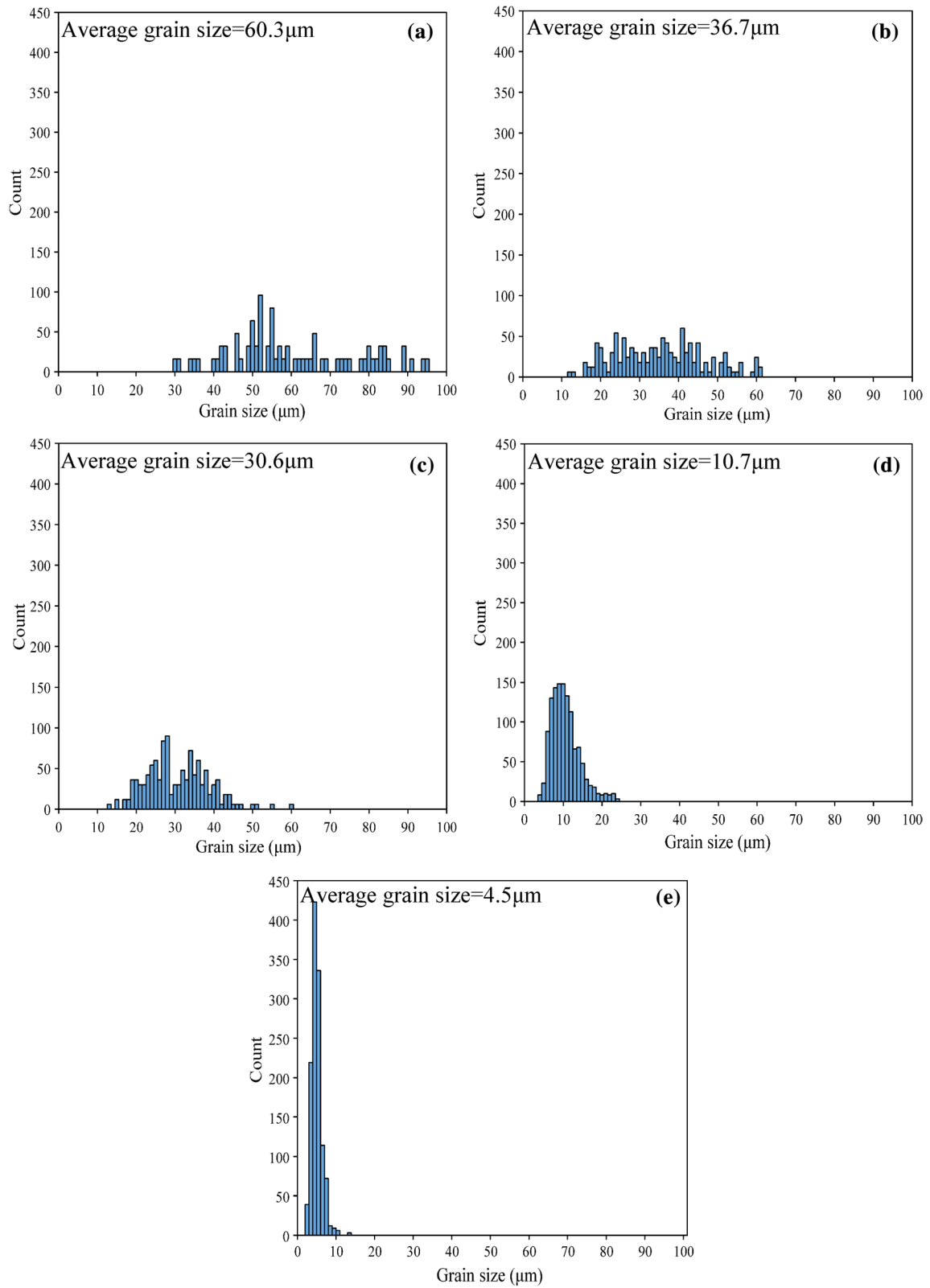


Fig. 5 Grain size distribution of the **a** Annealed AZ80, **b** Annealed SiC/AZ80, and the SiC/AZ80 after **c** 1, **d** 3, **e** 5 passes of DECEL

grains and homogeneous microstructure (Figs. 4e and 5e). The average grain size after the fifth pass is $4.5\ \mu\text{m}$ and comparing Fig. 5d and e shows a significant growth in the microstructure homogeneity. The decrease in the reduction rate of the grain size with an increase in the number of the DECLE passes shows that the DRX process is reaching to its final stages. Strengthening AZ80 alloy with the 1.5 percent volume of sic. nanoparticles as a first step had a significant reduction of grain size by 39% compared to AZ80, and after applying five DECLE passes on SiC/AZ80 nanocomposite as the final step, a 92.5% decrease in grain size compared to AZ80 magnesium alloy (without nanoparticles) was observed.

The results of EDS Mg K, C K, and Si K analyses and the TEM image of sic. nanoparticles are presented in Fig. 6. Due to the presence of robust Van der Waals forces, nanoparticles tend to accumulate near each other.

The accumulation zones for nanoparticles are often weak points in the nanocomposite structures due to the lack of proper bonds between the matrix and the reinforcement phase. Therefore, there are a suitable location for the formation of the cracks. Furthermore, due to stress concentrations in these areas, the possibility of the fracture increases. This matter means that improving the properties of the nanocomposites is significantly dependent on the homogeneous and suitable distributions of the strengthening nanoparticles in the metal matrix. In this study, according to Fig. 6b and c, the homogeneous distribution of the nanoparticles, and lack of agglomeration can be observed after the stir casting process. According to Fig. 6d, which shows the transmission electron microscopy image of sic. nanoparticles, the nearly spherical geometry of these particles is well visible.

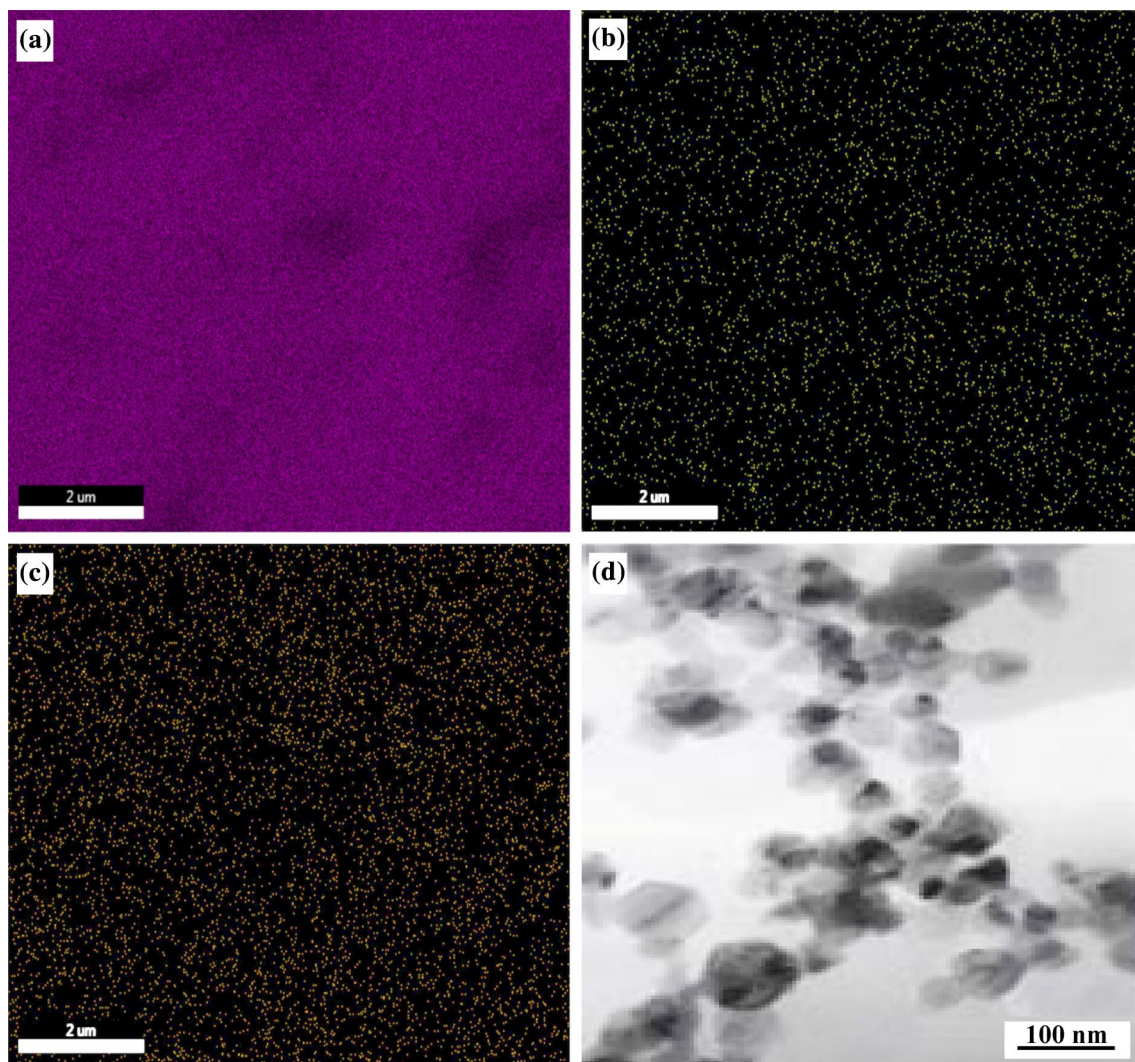


Fig. 6 EDS analysis of SiC/AZ80 magnesium matrix nanocomposite of **a** Mg K, **b** Si K, **c** C K and TEM image of sic. nanoparticles **d**

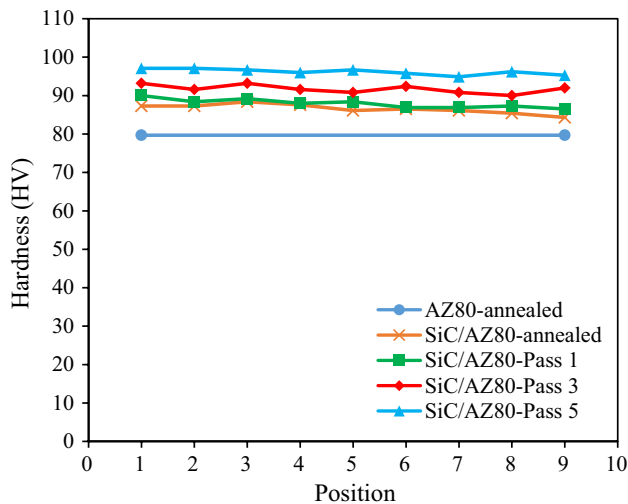


Fig. 7 The results of microhardness distribution on cross-section of billets

3.2 Microhardness Measurement

The results of the microhardness measurements at nine different points on the cross-section surface of AZ80 alloy and AZ80/SiC nanocomposites before and after the DECLE process are presented in Fig. 7. The cross-section used for these tests in the DECLE samples was perpendicular to the extrusion direction. The average hardness of the AZ80 alloy and AZ80/SiC nanocomposites were measured to be 79.7 HV and 86.6 HV, respectively. The increase in hardness due to the addition of sic. nanoparticles is similar to the results reported by Matin et al. [25]. The first pass of the DECLE process resulted in a slight increase in the hardness to 88 HV. The hardness significantly increased after third and fifth DECLE passes to 91.7 HV and 96.2 HV, respectively. The most significant increase in the surface hardness was observed after the addition of nanoparticles by 8.6%, and in general, the hardness of the AZ80 alloy was increased by 20.7% after strengthening with sic. nanoparticles and five passes of the DECLE process. As can be seen in Fig. 7, the surface hardness shows an increasing trend due to the addition of sic. nanoparticles and with an increase in the number of the DECLE passes, which occurs along with a reduction in grain size in all samples. On the other hand, the hardness measured at different locations in each sample shows no significant differences which indicates two facts: first, is that during the manufacturing of the nanocomposites through the stir casting process, distribution of the nanoparticles has been suitably carried out and that the DECLE process has not resulted in the agglomeration of the reinforcement phase. Second is that the strain distribution due to the DECLE process has been uniform in each sample. An increase in the hardness due to a decrease in the grain size and increased

homogeneity of the microstructures was also reported in the study by Fakhari et al. [23] who used the DECLE process on AA5083 aluminum alloy and indicated the applicability of Hall-Petch equation [29]. In the study by Alsubaie et al. [30], AZ80 alloy underwent up to 10 passes of HPT process and increased in the surface hardness along with an increase in the number of passes as well as uniform microstructures were reported. The 20% increase in microhardness of AZ31 alloy after four passes of the ECAP process at a temperature of 200 °C along with a decrease in average grain size from 20.2 to 1.6 μm was also reported on another study [31].

As can be seen in Fig. 7, other than the aforementioned facts, it can also be said that in samples with 1, 3, and 5 passes of the DECLE process, the average hardness of three measurement points at the highest row is higher than the average of the middle three points which are again higher than the average for the lowest three points. This is similar to the results reported by Seifi and Kazemi [32] for ECAPed 6063 aluminum alloy at a constant temperature. They believed that the reason for this decreasing trend in surface hardness is the compression of the upper portion and stretching of the lowest part of the sample during the SPD process.

3.3 Investigating Tensile Behavior

The engineering stress-strain curves resulting from the uniaxial tensile tests at room temperature of AZ80 alloy and AZ80/SiC nanocomposites before and after 1, 3, and 5 passes of the DECLE process are presented in Fig. 8. The results of these tests also indicate significant effects of the reinforcement nanoparticles on the tensile properties of the samples similar to the results for microstructure and hardness variations. Accordingly, the YS and UTS increase from 74 to 131.8 MPa for AZ80 alloy to 113 and 221.9 MPa for AZ80/SiC nanocomposite. The addition of the nanoparticles

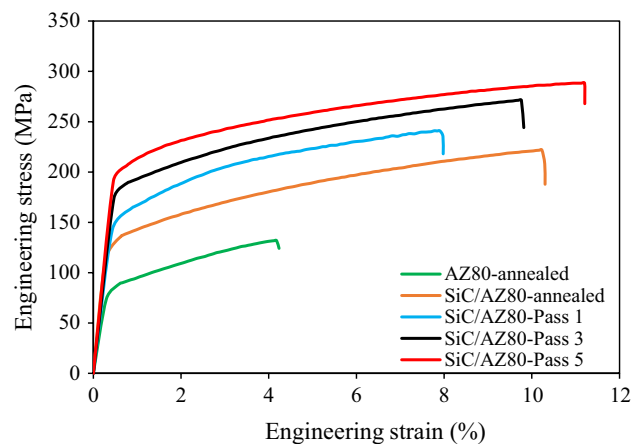


Fig. 8 The engineering stress-strain curves of room temperature tensile tests

not only increases the tensile strength but also improves ductility and has raised elongation from 4.2 to 10.3%. In general, improved strength as a result of the addition of the nanoparticles to the metal matrix is often accompanied by a drop in other properties such as ductility. However, this is not seen in the magnesium-based nanocomposites reinforced with the ceramic particles. This can be due to a decrease in the grain size, and its uniform distribution, activation of non-basal slip planes and changes in the crystalline texture [33]. The stress field created during the tensile test around smaller particles, which are the reinforcement, can be easily controlled through the distribution of the deformations, which delays the loss of the strength in the samples [34]. Simultaneous improvement in the strength and ductility in the magnesium-based nanocomposites have been reported in other studies using various volume fractions of the sic. nanoparticles [13, 26, 35, 36].

In total, factors contributing to the increased strength of the metal matrix after addition of the strengthening nanoparticles can be divided into the following categories:

- 1 Hall-Petch effect: This effect is based on the dislocation pileup in the grain boundaries and is also known as grain boundary strengthening effect. These pileups create stress concentration zones inside the grain boundaries, which are essential for the activation of the dislocation sources in adjacent grains and transfer of the dislocations between grains. Therefore, smaller grains restrict these pileups and thus limit the movement of the dislocations and increases tensile strength [37, 38]. As shown in Fig. 5a and b, in the current study, a 39% reduction in grain size after the addition of the strengthening particles is one of the main factors contributing to the increase in strength.
- 2 Orowan strengthening effect: During the collision between the dislocations and particles, dislocations are forced to loop around these obstacles before continuing their movements. This loop is known as the Orowan loop. This mechanism is not essential in composites strengthened with micro-sized particles due to a considerable distance between strengthening particle, which makes it easier for dislocations to loop around them. On the other hand, due to the small size of nanoparticles, this mechanism plays an essential role in nanocomposites [39]. Since the size of the nanoparticles used in the current study is small with an average size of 50 nm, the effect of the Orowan strengthening mechanism will become significant.
- 3 Effective load transfer effect: In the reinforcement phase, a higher specific ratio (the ratio of height to width of a shape) results in better load transfer from matrix to reinforcement, which results in a faster increase in strength. This ratio is smaller in spherical particles (Fig. 6d)

compared to other shapes (smaller than 1), therefore, compared to fiber or string composites, although those reinforced with particles are more uniform and isotropic, they don't create a significant improvement in the strength in terms of the effective load transfer [40].

- 4 Thermal mismatch effect: The difference in deformations of the matrix and strengthening phases due to variation in their thermal expansion coefficients, means that during temperature changes (including cooling after casting), the ceramic nanoparticles show significantly less deformation compared to matrix, preventing further deformation of the metal matrix and therefore create stress in the interface between these two phases. These stresses around the nanoparticles result in plastic deformations of the matrix and increase in the dislocation density, which then results in increased strength and hardness of the nanocomposites [41]. The thermal expansion coefficient of sic. nanoparticles is about $21.2 \times 10^{-6} \text{ K}^{-1}$ lower than that of AZ80 alloy [25]; therefore, the amount of induced thermal stresses will be significant.

The YS, UTS, and elongation values obtained from the stress-strain curves of all five samples are presented in Table 1. According to these results, the first pass of the DECLC process increases the tensile strength of the sample while decreasing its ductility in compared with the annealed nanocomposites. The increase in the tensile strength along with a decrease in the elongation in the first pass of the DECLC process on AZ31 alloy and the first pass of MDF process for SiC/AZ91 nanocomposites has also been reported in the literature [13, 20]. After the third pass, along with an increase in YS and UTS values, the elongation also shows an increasing trend, which can be due to finer grains and decrease in the number of coarse grains. However, ductility is still lower than in the annealed AZ80/SiC nanocomposite. Finally, after the fifth pass of the DECLC process, the highest values for strength and ductility are observed. The YS, UTS, and elongation values for nanocomposite after five passes of the DECLC process are 159%, 119%, and 167% higher than those for AZ80 alloy, respectively. Based on the results of the tensile test, it can be said

Table 1 Room temperature tensile properties of AZ80 alloy and SiC/AZ80 nanocomposites after different DECLC passes

Sample	Yield strength (MPa)	Ultimate strength (MPa)	Elongation (%)
AZ80-annealed	74	131.8	4.2
SiC/AZ80-annealed	113	221.9	10.3
SiC/AZ80-Pass 1	142.8	241	8
SiC/AZ80-Pass 3	173.9	271.3	9.8
SiC/AZ80-Pass 5	191.3	288.3	11.2

that the increase in the strength along with an increase in the ductility has occurred which is a desirable result for the magnesium nanocomposites. The Hall-Petch equation indicates an inverse relationship between yield stress and the square root of the average grain size, and this effect is more significant in the metals with HCP structure such as magnesium due to the limited number of the slip planes [27]. Therefore, the decrease in grain size and increase in the homogeneity of the microstructure, which starts with the addition of the nanoparticles and continues until the fifth pass of the DECLE process is one of the main factors contributing to the increase in the tensile strength. Since the Hall-Petch equation also works for hardness, it can be used to explain the similar trends of the increase in the microhardness with the decrease in the grain size.

3.4 Fractography

The SEM images of the fracture surface of the tensile strength test samples are shown in Fig. 9. According to Fig. 9a, the presence of cleavage surfaces in the fracture cross-section of AZ80 alloy indicates the brittle nature of its fracture. The occurrence of this type of fracture in unworked magnesium alloys at room temperature is not unexpected and is due to the limited-slip planes in an HCP structure [42]. According to Fig. 9b, due to the addition of sic. nanoparticles, the cleavage fracture surfaces have decreased, but some are still observed next to dimples with various sizes. This bimodal structure of the fracture is also predictable due to the bimodal structure of AZ80/SiC nanocomposite. The dark and light parts of the image indicate the difference in depth, showing the plastic deformations of the surface and changing of the fracture mechanism from brittle to ductile. Figure 9c shows the fracture surface of the sample after one pass of the DECLE process, showing an increase in the number of the cleavage surfaces and a decrease in the ductility. After the third pass of the DECLE, the fracture cross-section shows small and large dimples next to each other, which shows a gradual change in the fracture behavior from brittle to ductile (Fig. 9d). According to Fig. 9e, after the fifth pass, with the decrease in the grain size, the number of small dimples increases. Noticeable depth differences in different zones are observed, and compared to the

other four samples; it has the highest ductile fracture effects. These results are very similar to the results of the tensile test provided in Table 1.

4 Conclusion

AZ80 magnesium alloy and AZ80/SiC nanocomposite before and after five passes of the DECLE process at constant temperature were investigated. The summary of the results regarding to the microstructures, hardness, and tensile strength are as follows:

- 1 The addition of nanoparticles as the strengthening phase decreases the average grain size from 60.3 to 36.7 μm while also creates a more homogenous microstructure.
- 2 Using the DECLE process on AZ80/SiC nanocomposite and increase in the number of passes up to 5 passes expands the recrystallization of the samples, gradually leading to an ultrafine grain and homogenous structure with an average grain size of 4.5 μm .
- 3 Along with the decrease in grain size and an increase in accumulated strain, the surface hardness increased from 79.7 HV in AZ80 alloy to 96.2 HV in AZ80/SiC nanocomposite after five passes of the DECLE process.
- 4 The results of the tensile test indicate that YS and UTS of the nanocomposites have shown a significant increase in compared with AZ80 alloy, which Hall-Petch effect, Orowan strengthening mechanism, and thermal mismatch effects being the most important mechanisms for this change.
- 5 Yield stress and ultimate tensile strength values of AZ80 alloy were 74 and 131.8 MPa, which increased to 191.3 and 288.3 MPa after strengthening with sic. nanoparticles and five passes of the DECLE process.
- 6 The highest amount of improvement in microstructure, hardness, and tensile strength is observed after the addition of the nanoparticles.

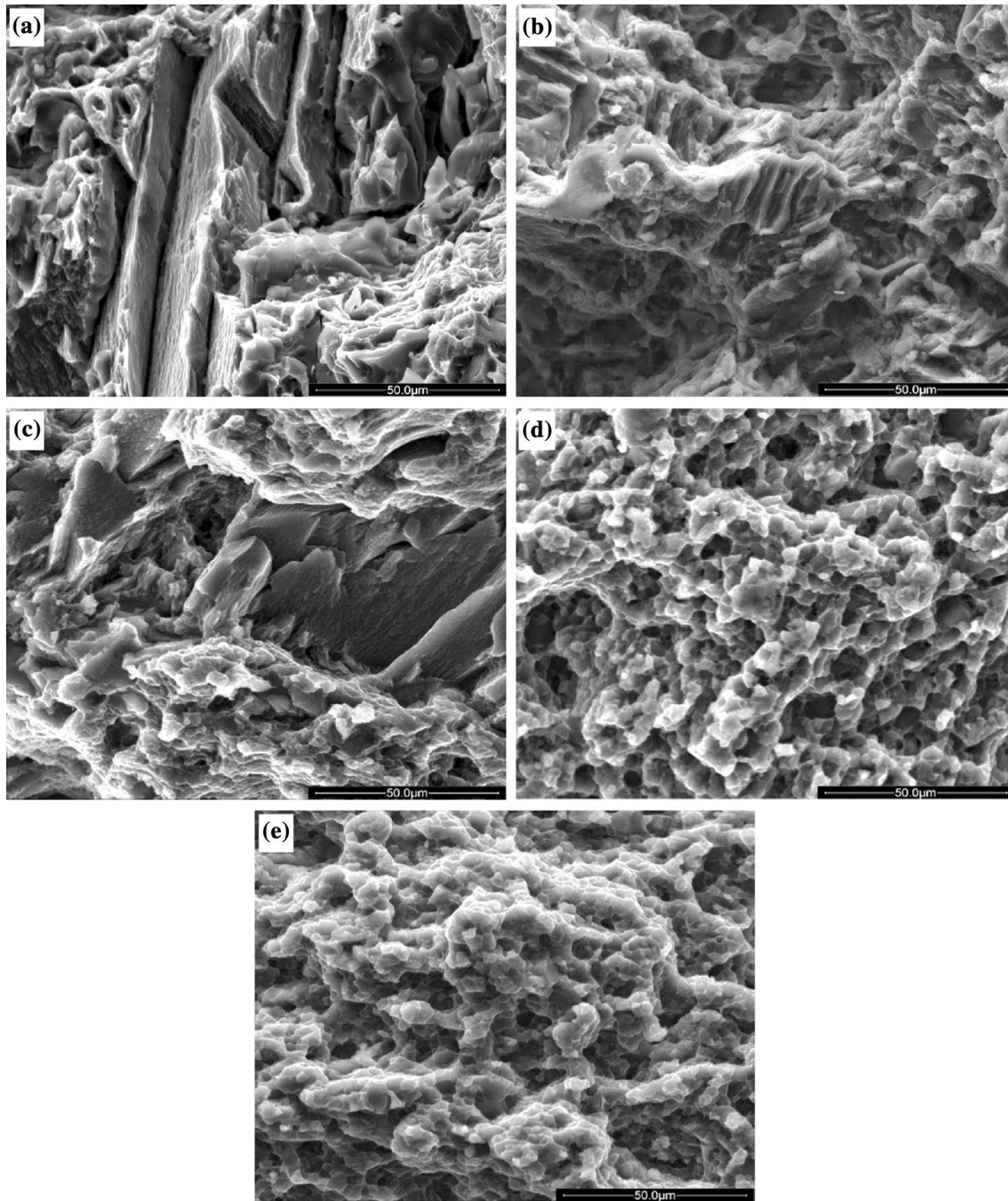


Fig. 9 SEM images of the fractured surfaces of the tensile test specimens for **a** the annealed AZ80, **b** the annealed SiC/AZ80, and the SiC/AZ80 after **c** 1, **d** 3, **e** 5 passes of DECEL

References

1. S. Huang, M. Lu, S. Luo, H. He, Y. Yi, *Met. Mater. Int.* (2019). <https://doi.org/10.1007/s12540-019-00452-7>
2. E. Maleki, F. Shahri, M. Emamy, *Met. Mater. Int.* **12**, pp. 1–13, (2019)
3. G. Yarkadaş, H. Şevik, *Met. Mater. Int.* (2019). <https://doi.org/10.1007/s12540-019-00560-4>
4. L. Chen, Y. Yao, *Acta Metall. Sin. (English Lett.)* **27**, 762 (2014)
5. K.K. Deng, J.C. Li, J.F. Fan, X.J. Wang, K. Wu, B.S. Xu, *Acta Metall. Sin. (English Lett.)* **27**, 885 (2014)
6. M. Gupta, W.L.E. Wong, *Mater. Charact.* **105**, 30 (2015)
7. B. Saleh, J. Jiang, A. Ma, D. Song, D. Yang, Q. Xu, *Met. Mater. Int.* (2019). <https://doi.org/10.1007/s12540-019-00491-0>
8. J. Zhao, J. Fu, B. Jiang, A. Tang, H. Sheng, T. Yang, G. Huang, D. Zhang, F. Pan, *Met. Mater. Int.* **19**, pp. 1–3, (2019)
9. J. Kubásek, D. Dvorský, J. Veselý, P. Minárik, M. Zemková, D. Vojtěch, *Acta Metall. Sin. (English Lett.)* **32**, 321 (2019)

10. Y. Huang, T.G. Langdon, *Mater. Today* **16**, 85 (2013)
11. V.V. Popov, E.N. Popova, *Mater. Trans.* **60**, 1209 (2019)
12. X.G. Qiao, T. Ying, M.Y. Zheng, E.D. Wei, K. Wu, X.S. Hu, W.M. Gan, H.G. Brokmeier, I.S. Golovin, *Mater. Charact.* **121**, 222 (2016)
13. K.B. Nie, K.K. Deng, X.J. Wang, T. Wang, K. Wu, *Mater. Charact.* **124**, 14 (2017)
14. W. Liao, B. Ye, L. Zhang, H. Zhou, W. Guo, Q. Wang, W. Li, *Mater. Sci. Eng. A* **642**, 49 (2015)
15. R.B. Figueiredo, T.G. Langdon, *Mater. Sci. Eng. A* **503**, 141 (2009)
16. S.M. Masoudpanah, R. Mahmudi, *Mater. Des.* **31**, 3512 (2010)
17. A. Heczal, F. Akbaripناه, M.A. Salevati, R. Mahmudi, A. Vida, J. Gubicza, *J. Alloys Compd.* **763**, 629 (2018)
18. B. Talebanpour, R. Ebrahimi, K. Janghorban, *Mater. Sci. Eng. A* **527**, 141 (2009)
19. B. Talebanpour, R. Ebrahimi, *Mater. Des.* **30**, 1484 (2009)
20. W. Guo, Q.D. Wang, B. Ye, M.P. Liu, T. Peng, X.T. Liu, H. Zhou, *Mater. Sci. Eng. A* **540**, 115 (2012)
21. F. Fereshteh-Saniee, N. Fakhar, F. Karami, R. Mahmudi, *Mater. Sci. Eng. A* **673**, 450 (2016)
22. Y. Iwahashi, J. Wang, Z. Horita, M. Nemoto, T.G. Langdon, *Scr. Mater.* **35**, 143 (1996)
23. N. Fakhar, F. Fereshteh-Saniee, R. Mahmudi, *Trans. Nonferrous Met. Soc. China* **26**, 3081 (2016)
24. ASTM E384-17, A.S.T.M. Int. West Conshohocken, PA (2017). <https://doi.org/10.1520/E0384-17>
25. A. Matin, F. Saniee, H.R. Abedi, *Mater. Sci. Eng. A* **625**, 81 (2015)
26. H. Khoshzaban Khosroshahi, F. Saniee, H.R. Abedi, *Mater. Sci. Eng. A* **595**, 284 (2014)
27. H.Z. Ye, X.Y. Liu, *J. Mater. Sci.* **39**, 6153 (2004)
28. V.V. Popov, E.N. Popova, A.V. Stolbovskiy, *Mater. Sci. Eng. A* **539**, 22 (2012)
29. J. Bai, F. Xue, S.N. Alhajeri, T.G. Langdon, *Mater. Sci. Forum* **667–669**, 391 (2010)
30. S.A. Alsubaie, Y. Huang, T.G. Langdon, *J. Mater. Res. Technol.* **6**, 378 (2017)
31. S.M. Masoudpanah, R. Mahmudi, *Mater. Sci. Eng. A* **526**, 22 (2009)
32. R. Seifi, M.A. Kazemi, *Fatigue Fract. Eng. Mater. Struct.* **41**, 1758 (2017)
33. S. Sankaranarayanan, R.K. Sabat, S. Jayalakshmi, S. Suwas, A. Almajid, M. Gupta, *J. Compos. Mater.* **49**, 3045 (2015)
34. P. Chen, Y. Sun, J. Jiang, A. Ma, Q. Lv, *Chinese J. Nonferrous Met.* **12**, 140 (2002)
35. W.L.E. Wong, M. Gupta, *Adv. Eng. Mater.* **8**, 735 (2006)
36. M. De Cicco, H. Konishi, G. Cao, H. Choi, L.-S. Turng, J.H. Perepezko, S. Kou, R. Lakes, X. Li, *Metall. Mater. Trans. A* **40**, 3038 (2009)
37. E.O. Hall, *Proc. Phys. Soc. Sect. B* **64**, p. 747, (1951).
38. N.J. Petch, *J. Iron Steel Inst.* **174**, 25 (1953)
39. Z. Zhang, D.L. Chen, *Scr. Mater.* **54**, 1321 (2006)
40. D.P. Mondal, N.V. Ganesh, V.S. Muneshwar, S. Das, N. Ramakrishnan, *Mater. Sci. Eng. A* **433**, 18 (2006)
41. Z. Zhang, D.L. Chen, *Mater. Sci. Eng. A* **483–484**, 148 (2008)
42. F.-D. Dumitru, O.F. Higuera-Cobos, J.M. Cabrera, *Mater. Sci. Eng. A* **594**, 32 (2014)

Publisher's Note Springer Nature remains neutral with regard to jurisdictional claims in published maps and institutional affiliations.